DOI 10.1007/s11182-023-03054-4
Russian Physics Journal, Vol. 66, No. 11, January, 2024

MICROSTRUCTURE AND STRENGTH OF A FRICTION STIR WELDED LOW-ALLOY STEEL PROCESSED BY TEMPFORMING

A. S. Dolzhenko,[1] A. S. Lugovskaya,[1] A. N. Belyakov,[1] and R. O. Kaibyshev[2] UDC 669.018.2

A feasibility of the friction stir welding for low-alloy structural steel processed by tempforming was analyzed. The stir zone was characterized by almost twofold increase in the hardness and the specific microstructure with an average grain size of 800 nm and large fractions of boundary misorientations around 60° and below 5°. The yield strength of the welded joint was 1220 MPa, whereas the yield strength of the base material was 1350 MPa. The fracture of the welded joint occurred in the heat affected zone between the stir zone and the base material.

Keywords: low-alloy steel, tempforming, microstructure, friction-stir welding, mechanical properties.

INTRODUCTION

High-strength low-alloy steels with a nanocrystalline lamellar microstructure resulted from a special thermomechanical treatment (tempforming), including large strain warm rolling at tempering temperature, have a unique combination of high strength (yield strength above 1000 MPa) and high impact toughness at low temperatures (KCV more than 100 J/cm^2 at 77 K) [1–5]. Such steels are promising materials for large scale products designed for structures operating at low temperatures and experiencing impact loads. High-strength steels are also used to create lightweight welded structures. Various welding technologies are used to join parts made of high-strength steels such as automatic, argon-arc welding, submerged arc welding, etc. [6–12].

The main difficulty in welding high-strength structural steels is their increased susceptibility to hardening, which leads to a sharp increase in hardness in the heat affected zones, which adversely affects the mechanical properties of welded joints. In addition, the welded seam and heat affected zone of welded joints obtained by traditional steel welding methods are characterized by a coarse-grained microstructure, which is an inevitable consequence of the melting of the welded material. This is completely unacceptable for the steels after tempforming, whose outstanding mechanical properties are due to the formation of a specific microstructure with a transverse grain size well below one micrometer. Unlike traditional welding methods, innovative friction stir welding (FSW), which is accompanied by a large plastic deformation of the welded material, makes it possible to obtain a welded joint with an ultrafine grain microstructure [13]. The aim of the present study was to analyze a feasibility of applying FSW for high strength low-alloy steels processed by tempforming. The mechanical properties of the FSW joint were evaluated by tensile test and discussed with close relation to the developed microstructure.

MATERIAL AND METHODS

A low-alloy steel with a chemical composition of Fe–0.36C–0.4Si–0.56Cr–0.57Mn–0.54Mo–0.0067P–0.0034S (all in mass%) was hot rolled at 1123 K followed by water quenching. Then the steel sample was tempered for 1 h at a temperature of 873 K followed by multiple rolling at the same temperature to a total strain of 1.5 (tempforming). After

[1]Belgorod National Research University, Belgorod, Russia, e-mail: dolzhenko_a@bsu.edu.ru; belyakov@bsu.edu.ru; [2]Russian State Agrarian University – Moscow Timiryazev Agricultural Academy, Moscow, Russia, e-mail: kajbyshev@rgau-msha.ru. Original article submitted November 27, 2023.

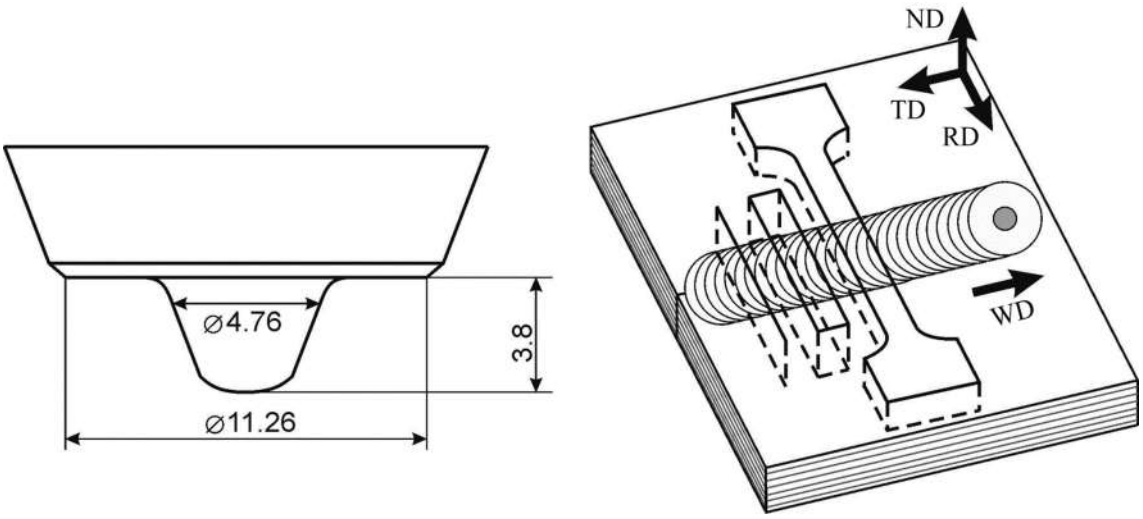

Fig. 1. Schematic drawing of the FSW tool and FSW joint.

tempforming, the steel sample was cut in two sheets with thickness of 4 mm. Next, the sheets were joined with FSW seam parallel to the transverse direction (TD) using an AccuStir 1004 FSW machine (General Tool Company). Attempting to provide a full-penetration joining, a double-side FSW technique was applied in mutually opposite directions such that the advancing side (AS) and retreating side (RS) reversed from the upper to the bottom surfaces of the weld. The welding process was performed using the tool with shoulder diameter of 11.26 mm and the cylindrical pin 3.8 mm in length and 4.78 mm in diameter (Fig. 1) made of tungsten carbide (WC). A tool rotation and travel speeds were 400 rpm and 100 mm/min, respectively. During FSW, the tool was tilted by 2.5° to the sheet normal such that the rear of the tool was lower than the front. The microstructural observations were performed on the RD-ND sections (RD is the rolling direction and ND is the normal direction) using a Quanta 600 FEG (FEI) scanning electron microscope (SEM) incorporating an orientation imaging microscopy (OIM) system (EDAX, Inc.). The SEM specimens were electro-polished using the electrolyte containing 10% perchloric acid and 90% acetic acid at a voltage of 20 V at room temperature. The OIM images were subjected to a clean-up procedure using the Grain Dilation method with Grain Tolerance Angle of 2° and Minimal Grain Size of 3. The mean grain and subgrain sizes were evaluated on the OIM images as average distances between high-angle boundaries (HAB) with misorientations of $\theta \geq 15°$ and low-angle sub-boundaries of $2° \leq \theta < 15°$, respectively. The tensile tests were carried out by using an Instron 5882 testing machine (Illinois Tool Works Inc.) on specimens with a gauge length of 25 mm and a cross-section of 7 mm × 3 mm at ambient temperature and a crosshead rate of 2 mm/min with the tensile direction parallel to the RD. The tensile specimens were machined crosswise to the welding direction (WD) and included all FSW microstructural zones. Vickers hardness was measured using a Wolpert 420MD tester at a load of 3 N and a holding time of 10 s. The measurements were carried out in the RD-ND section of the welded sample with a step between measured points of 0.5 mm, thus a hardness map and profile were obtained. The specimens for microstructural observation, tensile test, and hardness measurements are schematically shown in Fig. 1 together with their location in the FSW joint.

RESULTS AND DISCUSSION

The hardness distribution across the FSW joint along with the hardness change along the line starting in the base material and crossing the FSW seam is shown in Fig. 2. The hardness distribution clearly corresponds to the FSW seam, which in turn correlates with the pin trace during the second FSW pass (upper fragment of Fig. 2*a*). The stir zone is characterized by increased hardness, which is about two times higher than that of the base material equal to about 350 HV as obtained by tempforming. It should be noted that the first FSW pass, which could be observed in the bottom

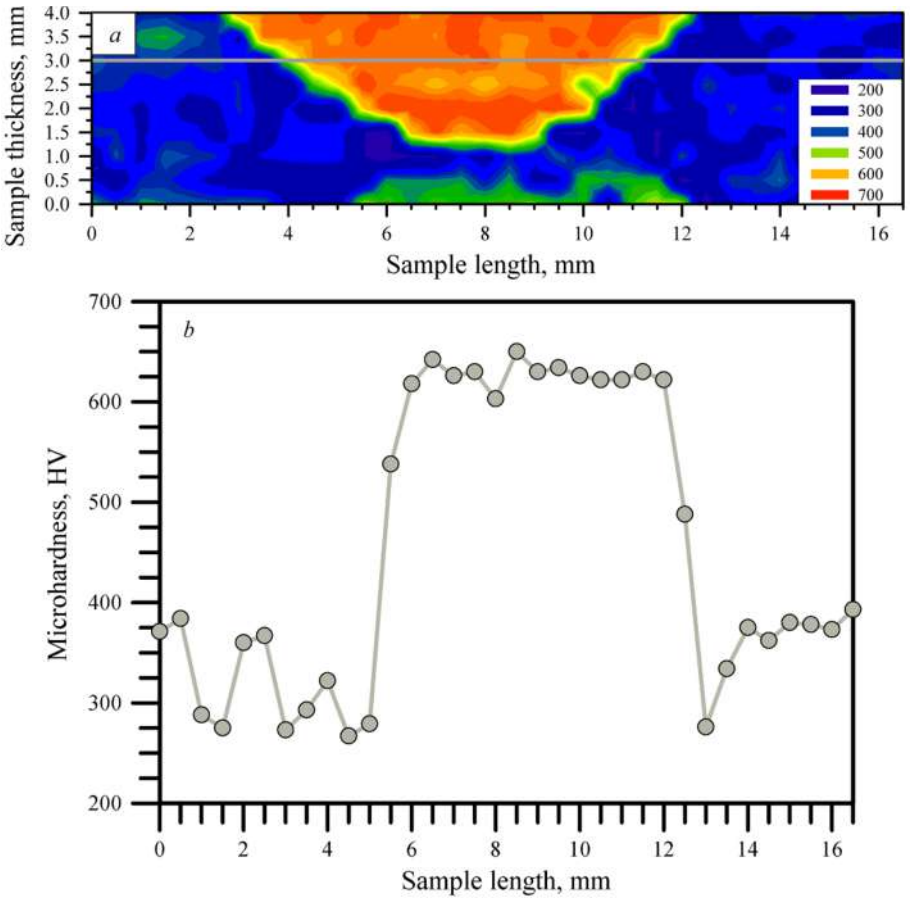

Fig. 2. Hardness mapping (*a*) and hardness change along the line across the stir zone of the FSW joint (*b*).

fragment of Fig. 2*a* is hardly revealed by the hardness mapping. A little increase in hardness can be only observed close to the bottom surface of the FSW sample in Fig. 2*a*. Therefore, it can be concluded that the hardening by the first FSW pass almost is completely removed by the second FSW pass. Another important point to be noted is a decrease in the hardness just between the base material and the FSW seam (Fig. 2*b*). This softening in the heat affected zone may have a serious consequence on the mechanical behavior of the FSW joint.

The representative microstructures evolved in the base materials and in the stir zone of the FSW sample are shown in Figs. 3*a* and 3*b*, respectively. The base material is characterized by a typical lamellar-type microstructure consisting of highly elongated grains with transverse grain size of 330 nm, which corresponds to that developed by previous tempforming at 873 K. In contrast, the microstructure evolved in the stir zone consists of fine irregular grains with frequently wavy/serrated boundaries. The mean grain size in the stir zone is 900 nm, which is about three times larger than that in the base material.

Such difference in the grain sizes suggests some recrystallization/grain coarsening processes taking place in the stir zone during FSW. The microstructural changes including grain growth may occur after austenite reversal due to temperature rise well above 1073 K that can be expected in the stir zone during FSW [12, 15].

The grain size distributions corresponding to the microstructures in the base material and the stir zone are shown in Figs. 4*a* and 4*b*, respectively. The base material is characterized by the grain size distribution with a relatively sharp peak in the ultrafine grained range and a huge tail towards large sizes up to 10 μm. The latter is associated with the grain sizes measured along the RD, i.e., the longitudinal size of highly elongated grains in the tempformed microstructure. In contrast, the ultrafine grains evolved in the stir zone are almost equiaxed. Except narrow peaks for

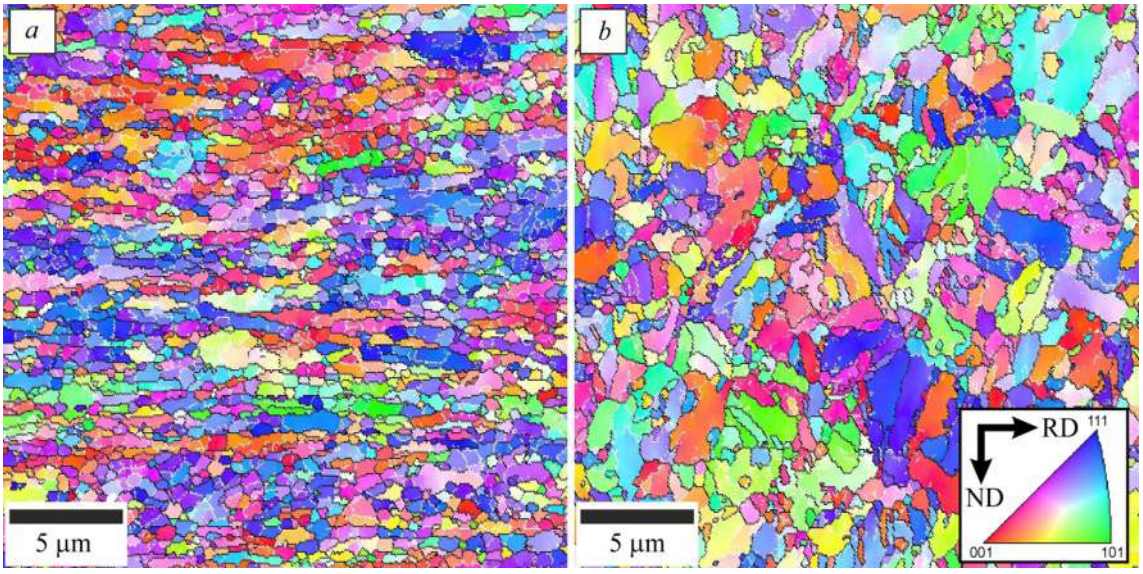

Fig. 3. Microstructures in the base material (*a*) and stir zone of the FSW joint (*b*).

grain sizes of about 100 nm, the grain sizes measured along the ND and RD in the stir zone exhibit almost normal distributions. Note here that the peaks corresponding to the smallest grain sizes may result from the insufficient quality of original electron backscattered diffractions (EBSD) that in turn are caused by the high density of internal defects in ultrafine grains/subgrains developed by large strain warm rolling (base material) and FSW (stir zone).

Figures 4*c* and 4*d* display the grain boundary misorientation distributions for the microstructures in the base material and stir zone, respectively. Note that the misorientation distribution for random disorientation of cubes [14] is also indicated by solid lines in these figures. The grain boundary misorientation distribution in the lamellar-type microstructure developed by large strain warm rolling (tempforming) in the base material is typical of ultrafine grained steels and alloys subjected to severe deformation [16, 17]. Namely, the misorientation distribution includes a sharp peak for low-angle subboundaries evolved by plastic deformation and large fraction of high-angle grain boundaries [16]. The latter ones include numerous strain-induced grain boundaries. The high-angle grain boundaries in metals and alloys subjected to severe plastic deformation are characterized by almost the same fractions of various misorientations, resulting in a flat-type misorientation distribution [16].

In contrast, the misorientation distribution in the stir zone of the FSW sample is differentiated by two remarkable peaks. One of them corresponds to low-angle subboundaries, while another stands for high-angle boundaries with misorientations of around 60°. Such misorientation distribution of grain boundaries and subboundaries with large fractions of low-angle subboundaries and high-angle boundaries with 60° misorientations testifies to martensitic origin of the microstructure evolved in the stir zone. Evidently, the steel in the stir zone was heated to austenite region during FSW followed by rapid cooling behind the FSW tool. The significant increase in the hardness in Fig. 2*b* also suggests the martensitic transformation in the stir zone just after FSW.

The developed textures for the base material and stir zone of the FSW sample are represented in Fig. 5 as the orientation distribution functions (sections of $\varphi_2 = 0°$ and $\varphi_2 = 45°$). The base materials processed by tempforming, i.e. warm rolling with large total reduction, exhibits remarkable γ-fiber (<111>//ND) with a maximum at {111}<110>, strong {223}<110>, and Rotated Cube ({001}<110>) in Fig. 5*a*. These texture components are typical of the body centered cubic (bcc) metals subjected to plate rolling [1, 18]. In contrast, the texture in the stir zone (Fig. 5*b*) includes rather strong Cube ({001}<100>) and Rotated Cube components. The development of such specific texture in spite of combined treatment including large deformation and phase transformations deserves more detailed investigation.

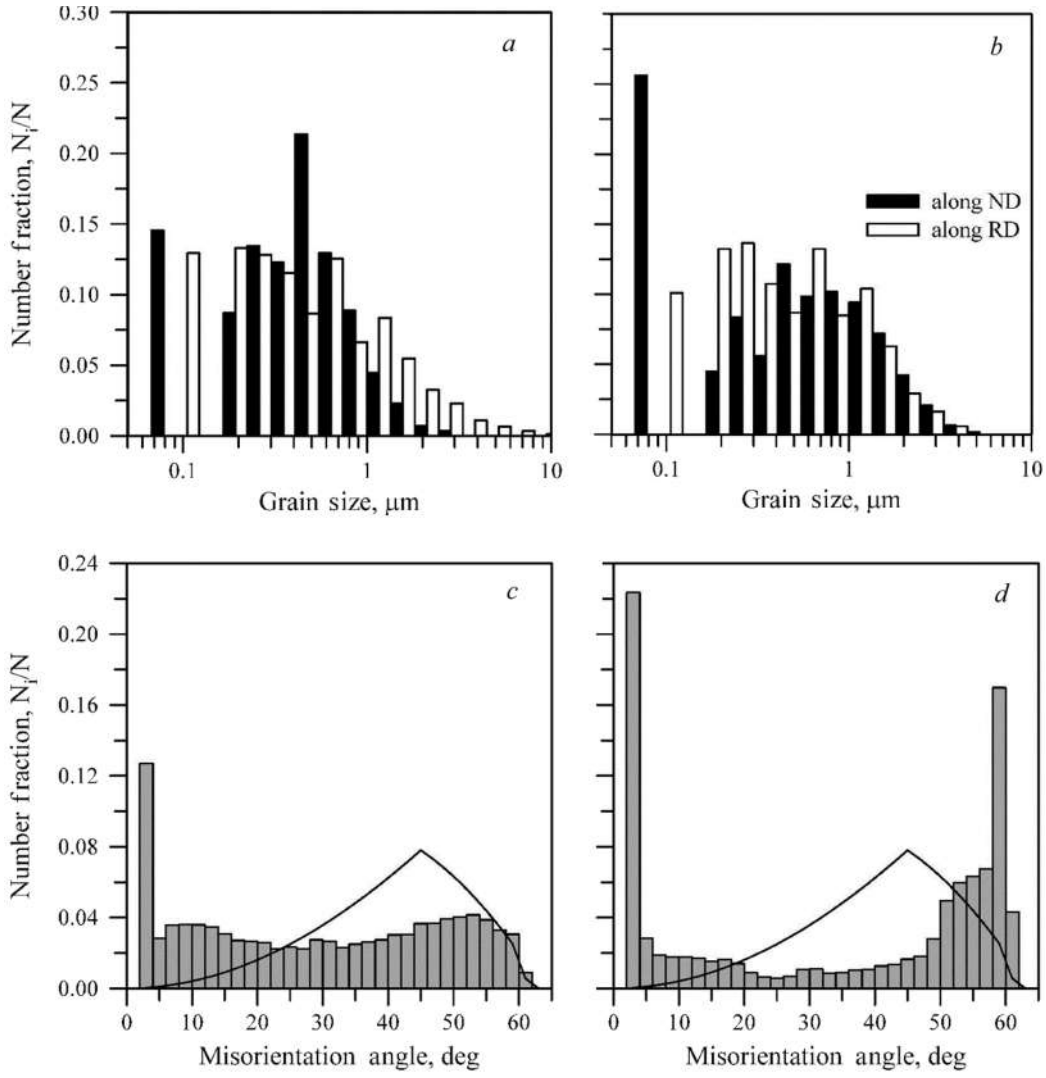

Fig. 4. Grain size distributions (*a* and *b*) and grain boundary misorientation distributions (*c* and *d*) in the base material (*a* and *c*) and stir zone of the FSW joint (*b* and *d*).

The FSW joint exhibits high strength comparable with that of the base material, which was work hardened by tempforming treatment. The tensile stress vs elongation curve of the FSW sample is shown in Fig. 6. The inserts in Fig. 6 show the corresponding fractured specimen and the tensile stress – elongation curve for the base tempformed material [1]. The yield strength of the FSW joint comprises 1220 MPa that is just below the yield strength of 1350 MPa as recorded by the base material after tempforming at 873 K [1]. However, in contrast to the base material, the FSW sample is characterized by a quite small plasticity. The total elongation for the specimen made of the FSW joint sample does not exceed 0.6% in Fig. 6. This specimen experienced rapid fracture localized in the heat affected zone, i.e. between the FSW seam and the base material (see insert in Fig. 6). This portion of the FSW joint demonstrates the lowest hardness (see the corresponding profile in Fig. 2*b*) and could be expected to be the preferred site for the strain localization upon tensile test. The stir zone experienced heating to the relatively high temperature above 1073 K during FSW. Then the martensitic transformation upon rapid cooling hardens the zone of the FSW seam. However, the neighboring portions of the FSW seam located close to the stir zone do not undergo phase transformation. Instead of hardening, the heat affected zone in the FSW joint softens due to the heat flux from the hot stir zone.

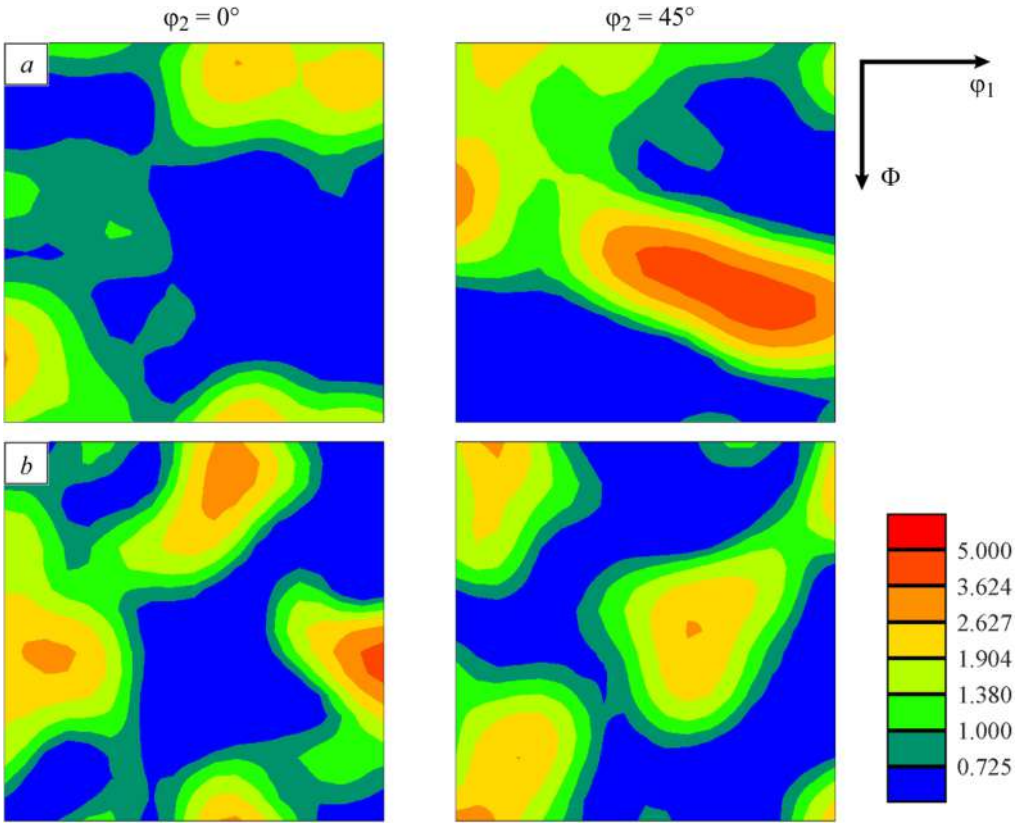

Fig. 5. ODF for the base material (*a*) and stir zone of the FSW joint (*b*).

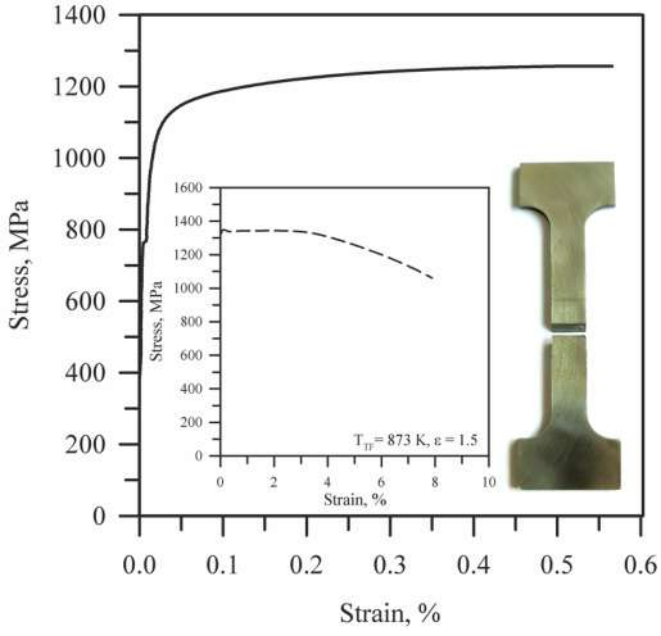

Fig. 6. Tensile stress-strain curve for the FSW joint specimen. Inserts show the tensile stress-strain curve for the base material [1] and the picture of the FSW joint specimen after tensile fracture.

CONCLUSIONS

The microstructures developed in the stir zone during FSW and the mechanical properties of the FSW joint of the high-strength low-alloy steel subjected to tempforming at 873 K have been studied. The main results can be summarized as follows.

The hardness leveled at about 350 HV for the base material increased above 600 HV in the stir zone. On the other hand, a decrease in the hardness down to 300 HV was observed in the heat affected zone between the stir zone and the base material. The microstructures developed in the stir zone were characterized by the mean grain size of 800 nm and the large fractions of grain boundary misorientations below 5° and around 60°, suggesting martensitic transformation upon cooling after FSW. The corresponding texture in the stir zone consisted of rather strong Cube and Rotated Cube components. The yield strength of the FSW joint was 1220 MPa, whereas the yield strength of the base material was 1350 MPa. The fracture of the FSW joint occurred in the heat affected zone between the stir zone and the base material. FSW was successfully used to join a high-strength low-alloy steel processed by tempforming with the joint strength comparable with the strength of base material.

COMPLIANCE WITH ETHICAL STANDARDS

Author contributions

A.S.D conceived, planned, and carried out the experiment; A.S.L. contributed to sample preparation, carried out the experiment; A.N.B. conceived the original idea, contributed to the analysis of the results and writing of the manuscript; R.O.K. supervised the project. All authors have read and agreed to the published version of the manuscript.

Conflicts of interest

The authors declare that they have no known competing financial interests or personal relationships that could have appeared to influence the work reported in this paper.

Funding

This work was supported by the Russian Science Foundation (Grant No. 20-19-00497-П).

Financial interests

The authors have no relevant financial or non-financial interests to disclose.

Institutional review board statement

Applicable.

Acknowledgments

The work was carried out using the equipment of the Joint Research Center of Belgorod State National Research University “Technology and Materials.”

REFERENCES

1. A. Dolzhenko, R. Kaibyshev, and A. Belyakov, Materials, **15**, 5241 (2022); DOI: 10.3390/ma15155241.
2. A. Dolzhenko and A. Belyakov, AIP Conf. Proc., **2509** (1), 020056 (2022).; DOI: 10.1063/5.0084752.
3. A. S. Dolzhenko, P. D. Dolzhenko, A. N. Belyakov, and R. O. Kaibyshev, Phys. Met. Metall., **122**, 1014 (2021); DOI: 10.1134/S0031918X21100021.
4. Y. Kimura, T. Inoue, F. Yin, and K. Tsuzaki, Science, **320**, 1057 (2008); DOI: 10.1126/science.1156084.
5. Y. Kimura and T. Inoue, ISIJ Int., **60**, 1108 (2020); DOI: 10.2355/isijinternational.ISIJINT-2019-726.
6. V. Sampath, J. Kehl, C. Vizza, *et al.*, J. Mater. Eng. Perform., **17**, 808 (2008); DOI: 10.1007/s11665-008-9236-2.
7. S. Mukhopadhyay and T. K. Pal, Int. J. Adv. Manuf. Technol., **29**, 262 (2006); DOI: 10.1007/s00170-005-2510-7.
8. S. D. Bhole and A. G. Fox, Can. Metall. Q., **35**, 151 (1996).
9. L. Lan, X. Kong, C. Qiu, and D. Zhao, Mater. Des., **90**, 488 (2016); DOI: 10.1016/j.matdes.2015.10.158.
10. D. V. Kiran, B. Basu and A. De, J. Mater. Process. Technol., **212**, 2041 (2012); DOI: 10.1016/j.jmatprotec.2012.05.008.
11. J. Li, S. S. Nayak, E. Biro, *et al.*, Mater. Des., **52**, 757 (2013); DOI: 10.1016/j.matdes.2013.06.021.
12. R. Oyyaravelu, P. Kuppan, and N. Arivazhagan, J. Adv. Res., **7**, 463 (2016); DOI:10.1016/j.jare.2016.03.005.
13. R. Ramesh, I. Dinaharan, R. Kumar, and E. T. Akinlabi, Mater. Sci. Eng. A, **687**, 39 (2017); DOI: 10.1016/j.msea.2017.01.050.
14. J. K. Mackenzie, Biometrika, **45**, 229 (1958).
15. L. Y. Wei and T. W. Nelson, Mater. Sci. Eng. A, **556**, 51 (2012); DOI: 10.1016/j.msea.2012.06.057.
16. A. Dolzhenko, A. Pydrin, S. Gaidar, *et al.*, Metals, **12**, 482021 (2022); DOI: 10.3390/met12010048.
17. A. Belyakov, Y. Kimura, Y. Adachi, and K. Tsuzaki, Mater. Trans., **45**, 2812 (2004); DOI: 10.2320/matertrans.45.2812.
18. L. A. I. Kestens and H. Pirgazi, Mater. Sci. Technol., **32**, 1303 (2016); DOI: 10.1080/02670836.2016.1231746.